Available online at www.sciencedirect.com

ScienceDirect

journal homepage: www.elsevier.com/locate/issn/15375110

Research Paper

Quantification of petal patterns and colours of genus *Sinningia* (GESNERIACEAE)

Tzu-Ting Hung [1], *Hao-Chun Hsu* [1], *Yan-Fu Kuo* [*]

Department of Biomechatronics Engineering, National Taiwan University, Taipei, Taiwan

ARTICLE INFO

Article history:
Received 6 January 2020
Received in revised form
4 May 2020
Accepted 10 July 2020

Keywords:
Flower colour
Fully convolutional network (FCN)
Petal pattern
Sinningia

Plants belonging to genus *Sinningia* are popular ornamental plants with diverse petal patterns and fascinating petal colours. The patterns and colours of petals are crucial horticultural properties that determine a plant's commercial value. Generally, the patterns and colours of petals are evaluated by experienced horticulturalists. However, manual evaluation can be subjective and the decision criterion could fluctuate due to fatigue. This work proposed a method to automatically quantify the petal patterns and colours by investigating 11 species of *Sinningia*. The images of the ventral petal of flower specimens were captured using flatbed scanners. The regions of interest (ROI) were defined and segmented from ventral images. Subsequently, a fully convolutional network was applied to the ROI for automatically segmenting variegated parts (i.e., spots, strips, and plaques) from the background. The patterns and colours of petals were then analysed. The proposed method can be used for the automation of petal pattern rating, which generally is performed using naked-eye observations.

1. Introduction

Genus *Sinningia* (subtribe Ligeriinae, family Gesneriaceae) exhibits a high level of diversity in petal patterns and colours (Perret et al., 2007, Fig. 1). The species in the genus are popular ornamental plants. Petal patterns and colours contribute to the commercial value of ornamental plants and are the main object of the breeding trait of petals. Generally, the floral patterns and colours are described and evaluated using naked-eye examination based on test guidelines provided by the international union for the protection of new varieties of plants (UPOV, 2015). In the guidelines, the patterns of spots, stripes, and plaques in petals are described as key characteristics (Fig. 1). The colours are determined by comparing the reference colours provided in the royal horticultural society (RHS) colour chart. However, naked-eye examination could be subjective and the criterion between phenotypic states would fluctuate due to fatigue (Voss, 1992). Additionally, naked-eye examination causes the lack of accuracy in trait quantification.

Image-based methods, by contrast, are objective and reliable. These methods can quantify petal patterns and colours with high precision. Image-based methods have been used to quantify petal traits in studies. Inthiyaz et al. (2017) identified the petal texture of ten species in the Oxford dataset using

* *Corresponding author*. Department of Biomechatronics Engineering, National Taiwan University, No. 1, Sec. 4, Roosevelt Rd., Taipei, 106, Taiwan. Fax: +886 2 23627620.
E-mail address: ykuo@ntu.edu.tw (Y.-F. Kuo).
[1] These authors have contributed equally to this work.
https://doi.org/10.1016/j.biosystemseng.2020.07.008

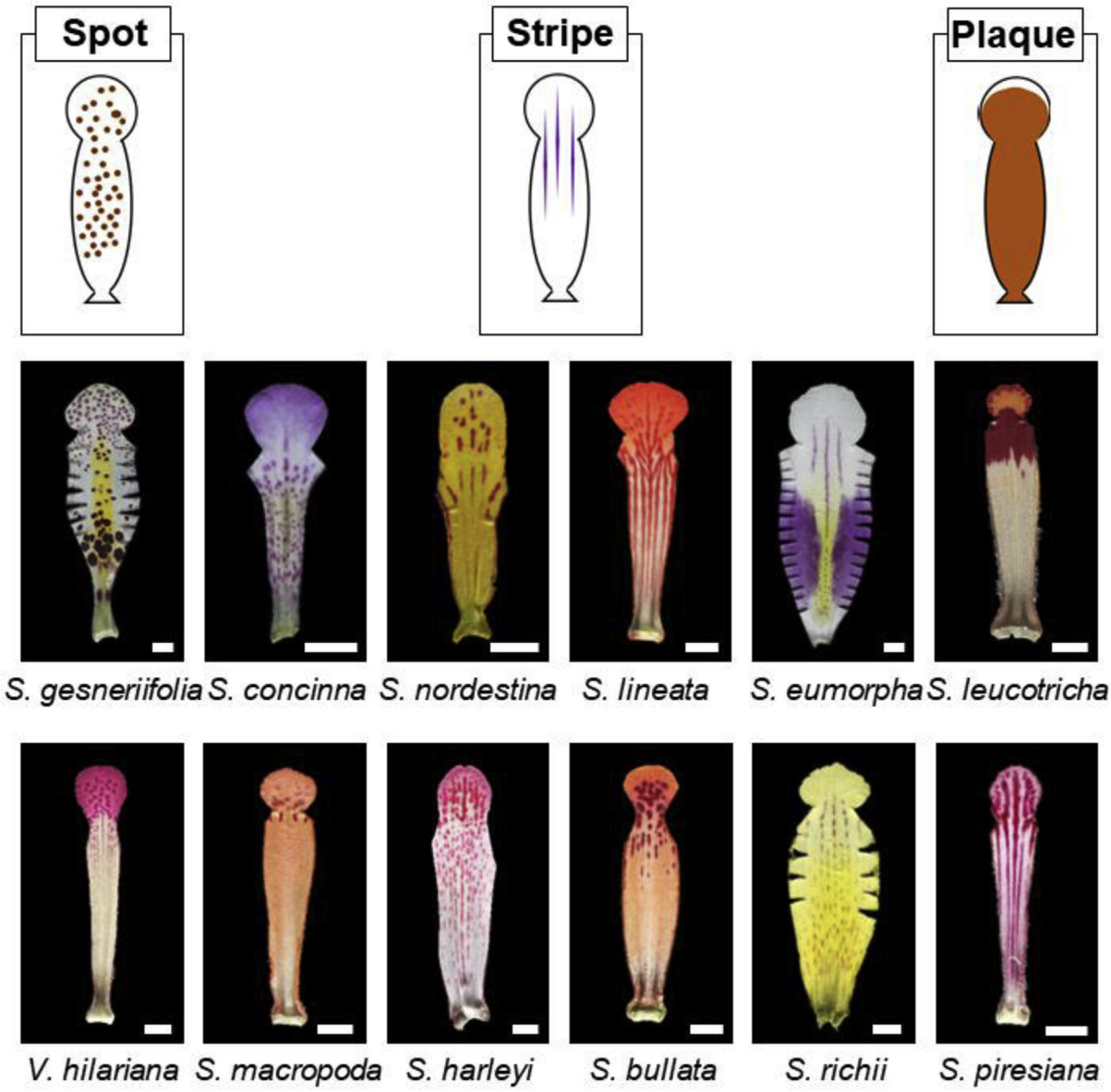

Fig. 1 – Ventral petals of 11 *Sinningia* and 1 *Vanhouttea* species. Scale bar: 0.5 cm.

local binary patterns (Guo et al., 2010). Hsu et al. (2018) quantified the spot and colour traits of *Sinningia speciosa* by employing a grey-level co-occurrence matrix (Haralick & Shanmugam, 1973). Yoshioka et al. (2006) analysed the picotee colours of *Lisianthus* petals and evaluated associations between colours and environmental factors. Koski and Ashman (2013) assessed the colour of *Argentina pacifica* flowers using ultraviolet spectra. De Keyser et al. (2013) studied the petal colours of *Rhododendron simsii* hybrids in both the red, green, and blue (RGB) and hue, saturation, and value colour spaces. Garcia et al. (2014) investigated the floral colours of eight species located at the campus of Monash University and obtained crucial physical characteristics using the colours of the flowers. Kendal et al. (2013) assessed the petal colours of 11 grassland species in CIE L*a*b* colour space (Hanbury & Serra, 2001).

Petal pattern segmentation, a process of separating the areas of petal patterns from its background, is essential for pattern and colour quantification. Generally, Otsu's thresholding (Otsu, 1979) is used for image segmentation. Although the method performed properly in many studies, manual adjustment was required to attain reasonable segmented results (See the studies of Patil & Shaikh, 2016; Biradar & Shrikhande, 2015; and Najjar & Zagrouba, 2012 for the details). Moreover, the petal patterns of genus *Sinningia* include various colours and are complex and diverse (Fig. 1). The background colour of certain petals also exhibits a gradient property (e.g., *S. concinna* and *S. bullata*).

Recently, fully convolutional networks (FCNs; Long et al., 2015) were proposed for segmenting complex images. FCNs are multilayer perceptrons composed of neurons to perform spatial convolution. After training the parameters of neurons,

FCNs can be employed to classify pixels in an image as foregrounds (i.e., petal patterns) or backgrounds with almost no preprocessing. FCNs are applied in the agriculture field. Iljazi (2017) segmented lettuce plants from the background and predicted the growth of the lettuce using the FCN with the DeconvNet architecture (Noh et al., 2015). Lameski et al. (2017) segmented carrot-weed in soil images using FCNs with the SegNet architecture (Badrinarayanan et al., 2015). Chen et al. (2018) identified and counted aphid nymphs on leaves using FCNs with the U-net architecture (Ronneberger et al., 2015). A study distinguished between crops and weeds in a field employing FCNs with the VGG16-U-net architecture (Fawakherji et al., 2019).

This study proposed a novel method to quantify the patterns and colours of petals. Petals could be classified into categories (e.g., spots, "spots and stripes", stripes, stripe and plaques, and plaques; Table 1) using the quantified traits. The proposed method is automatic and objective. Thus, it reduces the labour of phenotyping petal patterns and colours, and prevents inconsistency in phenotyping due to human fatigue. The framework of the proposed method is shown in Fig. 2. Ventral petals of fresh flowers were first scanned. The regions of interest (ROI) that contained petal patterns and colours were semiautomatically determined (Fig. 2a). Subsequently, an FCN was developed and used to automatically segment patterns (Fig. 2b) from the background (Fig. 2c). The pattern and colour traits (Fig. 2d) of the ROI were then defined and quantified using image-processing algorithms.

2. Materials and methods

2.1. Floral materials

A total of 11 species of genus *Sinningia* and a closely related species, *Vanhouttea hilariana*, with variegated petal patterns were included in this study (Table 1, Hung et al., 2019). The living flower specimens were collected from Dr. Cecilia Koo Botanic Conservation Center (KBCC). The plants were cultivated in a greenhouse at the KBCC under 22–28 °C, 70%–80% humidity, and sunlight. All the plants yielded corollas of five petals with variegation (i.e., petals with patterns of spots, stripes, or plaques). The corolla specimens of the species were collected at the full bloom stage. More than 10 corolla specimens were collected for each species, resulting in a total of 392 specimens.

2.2. Acquisition of the ROI

The ROI in the ventral petals of the specimens were acquired. The corolla was removed from a peduncle. Two lateral petals were dissected along primary veins and the remaining lateral lobes were removed to obtain the ventral petal (Fig. 3a and b). The image of the ventral petal was then captured using flatbed colour scanners (V37, Epson; Suwa, Japan) at a resolution of 600 dpi (Fig. 3c). The petal was flattened during scanning to maintain its original shape and was covered using a black cloth to prevent stray light from entering. The acquired image

Table 1 – *Sinningia* species accessions used in this study with the number of specimens and KBCC number.

Species	Number of specimens	Pattern type	KBCC number
S. bullata	38	Spot and Stripe	K039111
S. concinna	34	Spot	K039117, K039118
S. eumorpha	31	Stripe	K039132, K039133
S. harleyi	14	Spot and Stripe	K039135
S. leucotricha	36	Plaque	K039152, K039153, K039157
S. lineata	47	Spot and Stripe	K011972, K011973, K011984, K011994
S. macropoda	33	Stripe	K023363, K023375, K023403, K012405, K023413
S. nordestina	78	Spot and Stripe	K039168
S. piresiana	22	Stripe and Plaque	K023329, K023337, K023339
S. richii	15	Spot and Stripe	K039174, K039176, K039177
V. hilariana	33	Spot	K039217, K039218
S. gesneriifolia	11	Spot	K039220, K039221

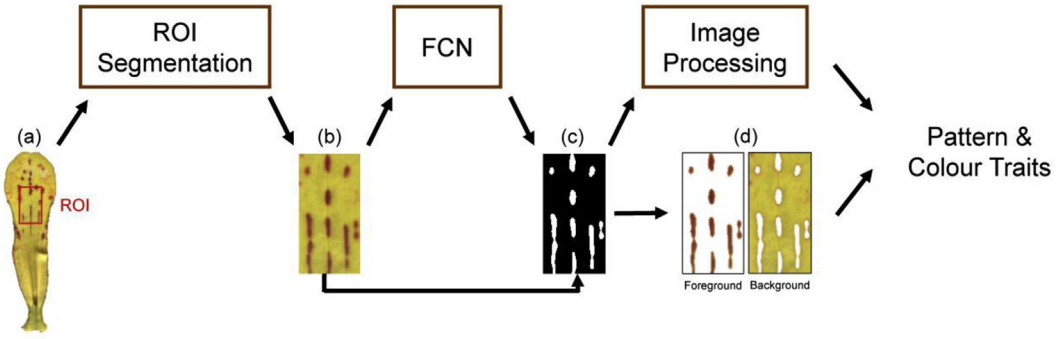

Fig. 2 – Quantification of petal patterns and colours: (a) petal and its region of interest (ROI), (b) ROI, (c) binary mask obtained using a fully convolutional network (FCN), and (d) patterns (foreground) and background.

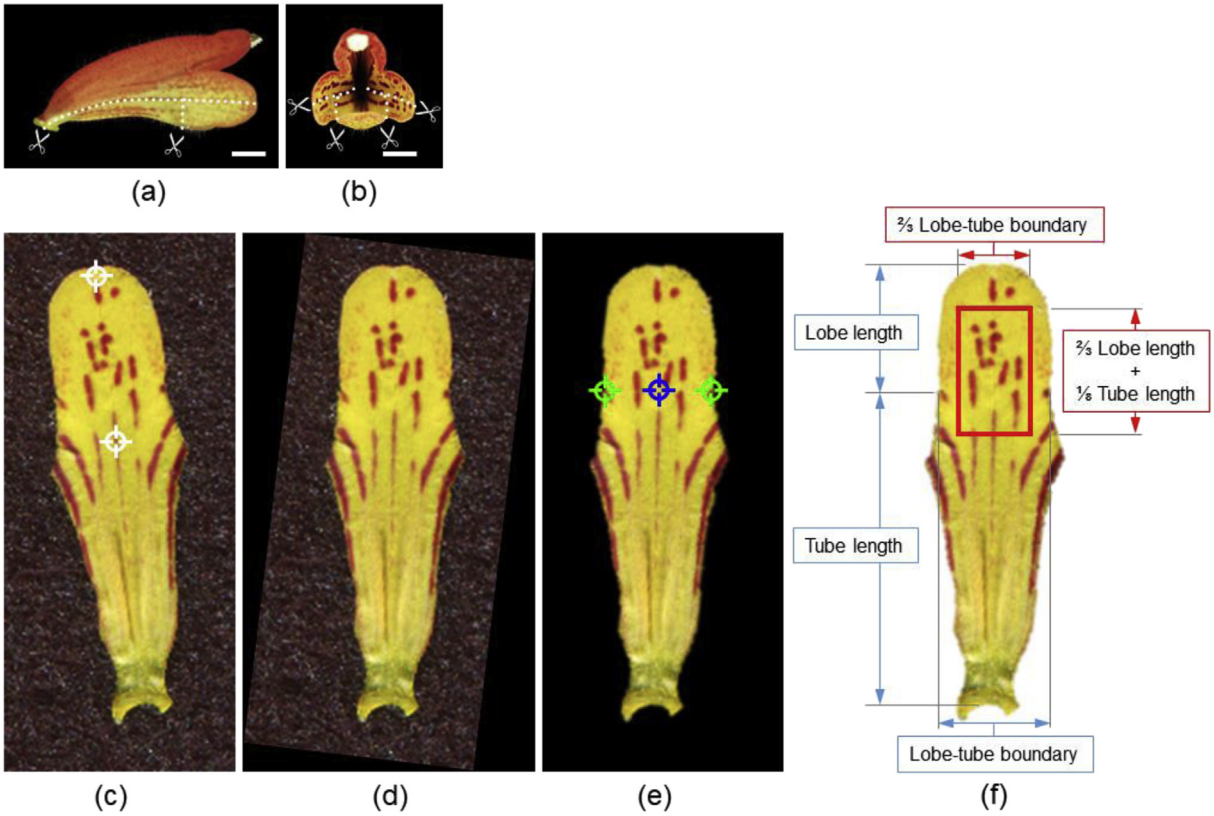

Fig. 3 – Acquisition of the region of interest (ROI) in the ventral petal: (a) side view of corolla, (b) front view of corolla, (c) annotation of the first-order vein (two white target symbols), (d) vertical alignment of the first-order vein, (e) background removal and annotation of the two endpoints (green target symbols) and centre (blue target symbol) of the lobe-tube boundary, and (f) definition of ROI (red rectangle). In (a) and (b), the white dotted lines denote the cutting lines of ventral petal dissection.

was then rotated for aligning the first-order vein of the petal with the vertical axis of the image (Fig. 3c and d). The background was removed using Gaussian-mixture-model-based segmentation (Nasios & Bors, 2006). Subsequently, the endpoints and centre of a lobe-tube boundary were manually annotated (Fig. 3e). The ROI was then automatically identified and obtained. The ROI was defined as a rectangle across the lobe-tube boundary and first-order vein of the ventral petal.

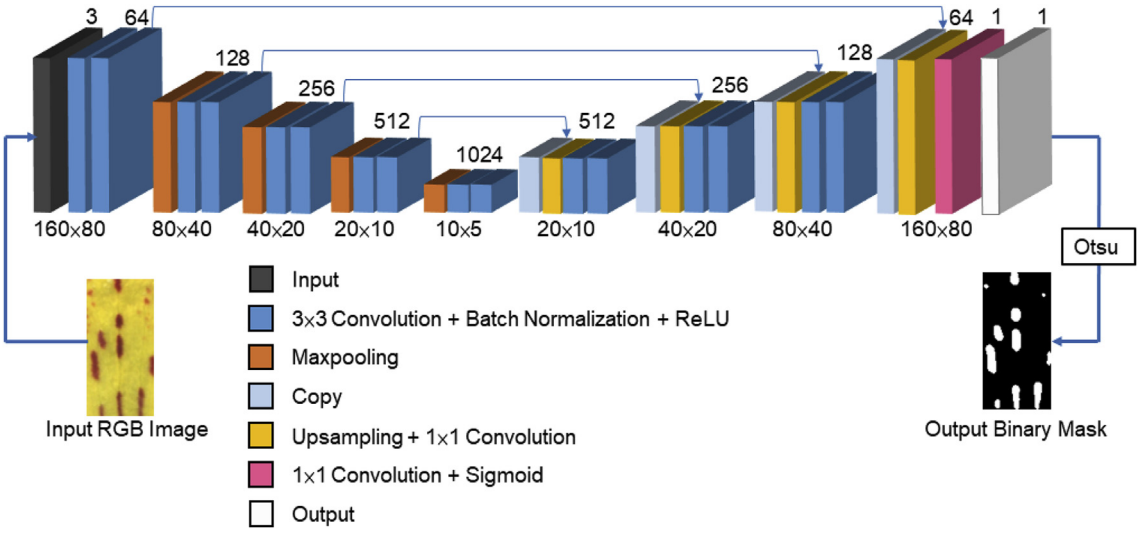

Fig. 4 – Architecture of the fully convolutional network (FCN).

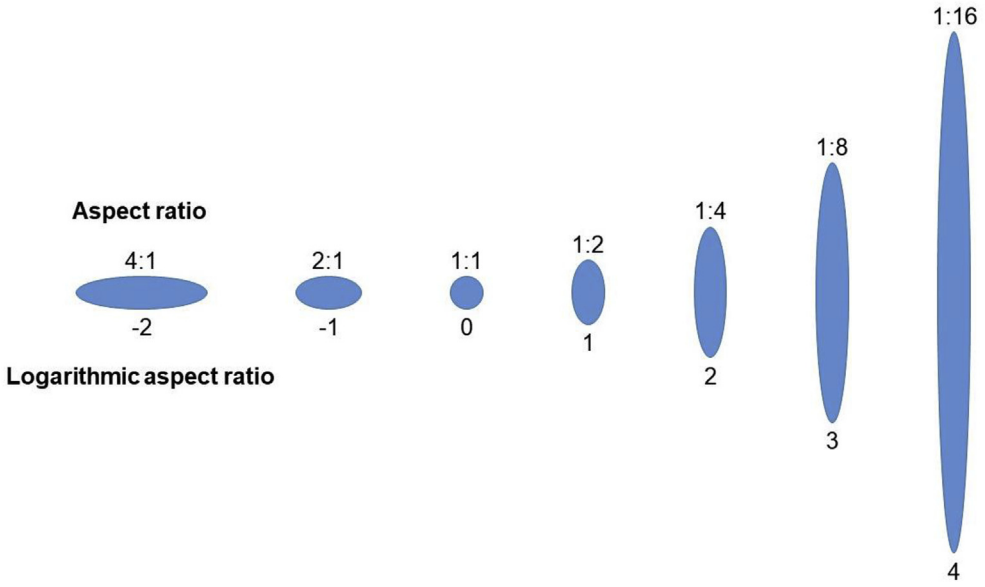

Fig. 5 – Illustration of aspect ratio and logarithmic aspect ratio of a spot or stripe.

The width of the ROI was two-third of the lobe-tube boundary. The height of the ROI was a summation of two-third of the lobe length and one-eighth of the tube length (Fig. 3f). The aforementioned procedures were implemented using MATLAB (The MathWorks; Natick, MA, USA).

2.3. *Segmentation of ROI patterns*

Patterns in the ROI were automatically segmented using an FCN (Fig. 4). The FCN architecture was adapted from U-net. The proposed network comprised eight repetitive structures, each of which had two convolutional layers with kernels of 3 × 3 pixels, a batch normalization (Ioffe & Szegedy, 2015), and a rectified linear unit (ReLU; Glorot et al., 2011). The first four repetitive architectures formed a contracting path, whereas the last four repetitive architectures formed an expanding path. In the contracting path, max pooling operations with kernels of 2 × 2 pixels were used for downsampling. In the expansion path, bilinear upsampling operations (Odena et al., 2016) were implemented, each of which followed by a convolutional operation with a kernel of 1 × 1 pixel. After a convolution operation, the resulting

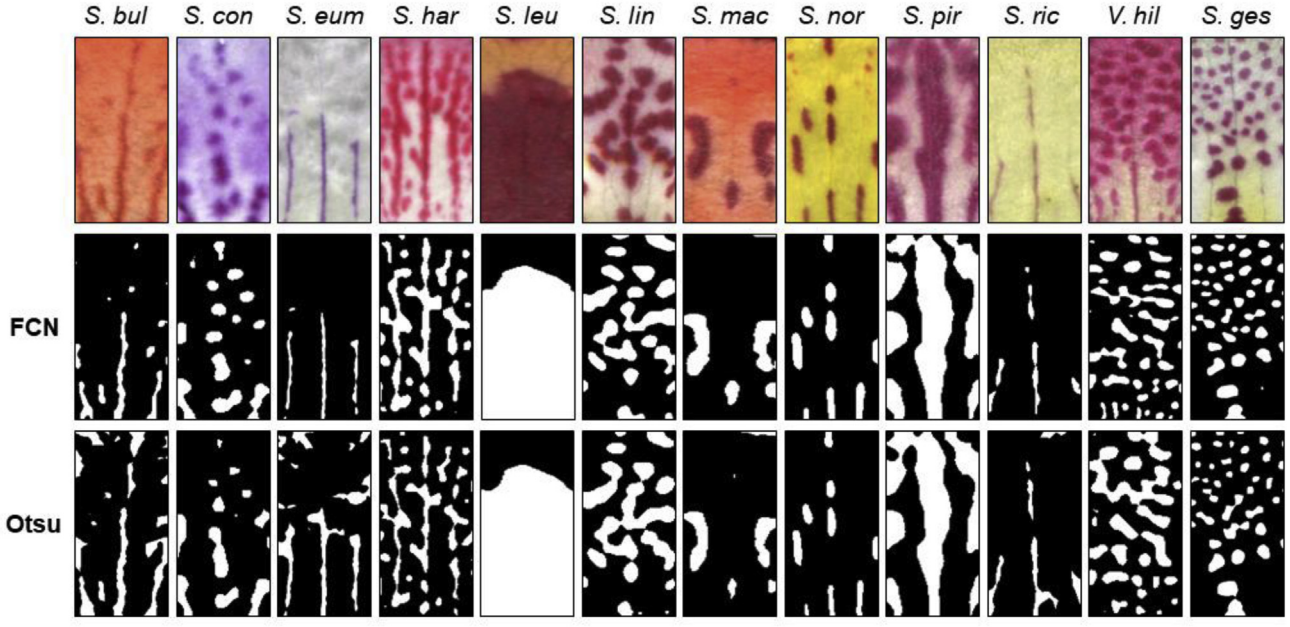

Fig. 6 – Pattern segmentation by using the fully convolutional network (FCN) and Otsu's algorithm.

Table 2 – Kruskal–Wallis test of pattern traits.

Pattern traits	*F* value	*p* value
Primary area ratio	1167.59	4.0735×10^{-285}
Secondary area ratio	306.10	3.2632×10^{-181}
Mean component	69.38	7.8938×10^{-84}
Component quantity	223.67	2.0038×10^{-158}

feature maps were concatenated with the feature maps from the corresponding layer in the contracting path. To make the feature map dimensions of the contracting and expanding layers consistent, zero-padding was applied to feature maps from the contracting path before the concatenation. The last layer of the FCN was a convolution operation with a kernel of 1×1 pixel followed by a sigmoid activation function. The resulting feature maps were then binarised using Otsu's thresholding to form binary masks containing patterns in the ROI.

For the FCN, 326, 33, and 33 ROI were used as the training, validation, and test samples, respectively. The ground-truth labelling of patterns in the training and validation samples was achieved using Otsu's thresholding, morphological erosion (Van Den Boomgaard & Van Balen, 1992), and manual labelling. The images were first resized to 150×75 pixels. Then reflection padding (Kitagawa et al., 2004, pp. 833–845) was applied to those images. The image size became 160×80 pixels. Augmentation was implemented to the resized training images for improving the robustness of the trained FCN. The augmentation operations included horizontal flipping, vertical flipping, rotation (randomly between $-10°$ and $10°$), height shift (randomly between -36 and 36 pixels), width shift (randomly between -16 and 16 pixels), zoom out (randomly between 0.9 and 1), and zoom in (randomly between 1 and 1.1). The FCN was trained for 80 epochs using adaptive moment estimation (Kingma & Ba, 2014) as the optimiser and binary cross entropy as the loss. The initial learning rate was set to 0.00002. Dropout (Srivastava et al., 2014) with a rate of 0.5 was applied to the last two max pooling operations to prevent the network from overfitting. The training was implemented using Python 3 and Pytorch toolbox (Paszke et al., 2017). A graphic processing unit (GeForce GTX 1080 Ti, NVIDIA; Santa Clara, USA) was used to expedite the training. The performance of FCN was evaluated using the Dice score (Dice, 1945):

$$\text{Dice score} = \frac{2|X \cap Y|}{|X| + |Y|}, \tag{1}$$

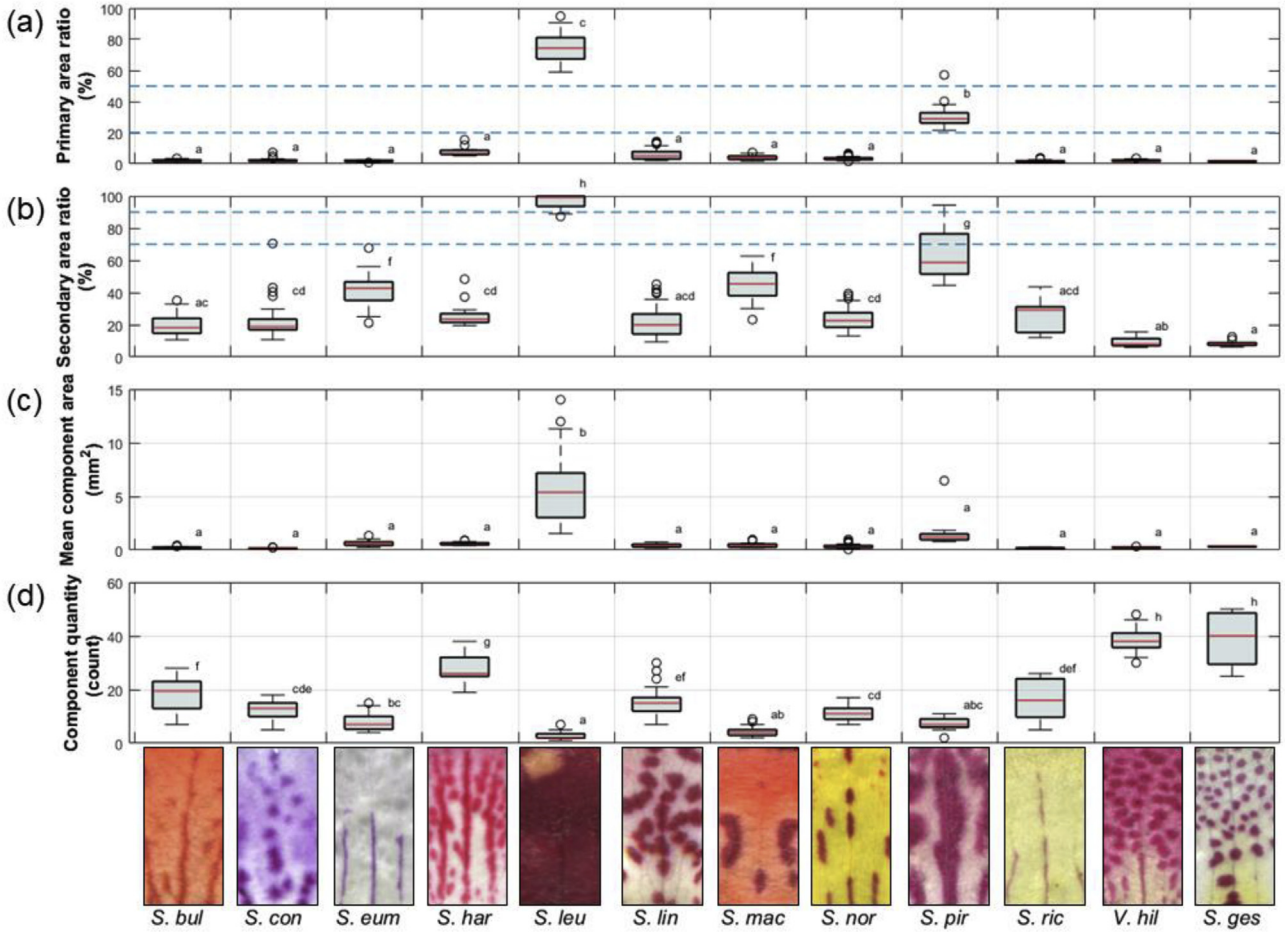

Fig. 7 – (a) Primary area ratio, (b) secondary area ratio, (c) mean component area, and (d) component quantity of *Sinningia* specimens. The lowercase alphabets placed at top right of box plots denote the groups of Scheffé's multiple comparison tests performed with a confidence level of 0.99.

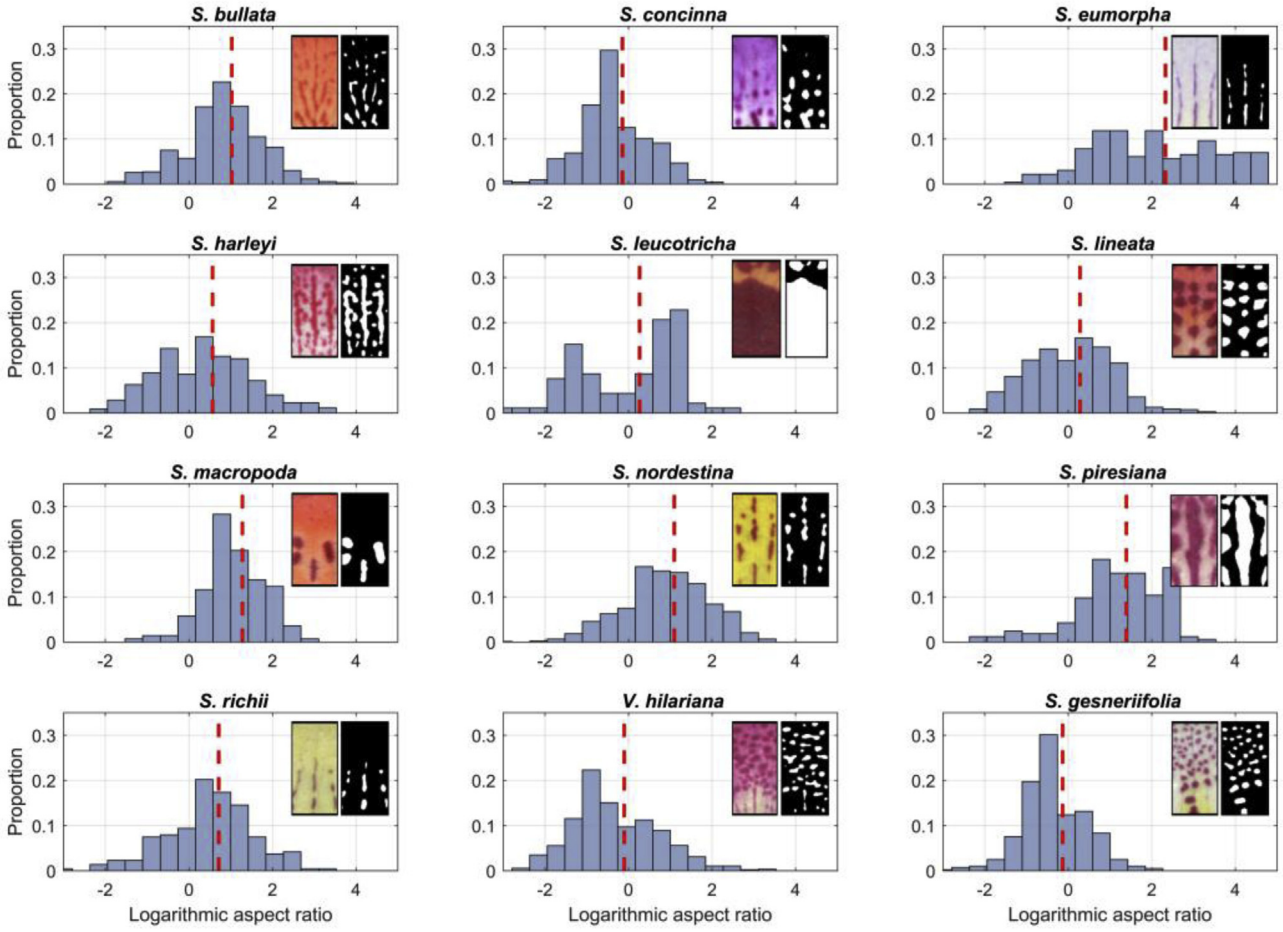

Fig. 8 – Distribution of logarithmic aspect ratio of the *Sinningia* species. The images placed at the right-top of each histogram denote the ROI (left) and FCN segmented pattern (right) of each species. The dashed lines represent the means of the logarithmic aspect ratios.

where X denotes the foreground pixels obtained from the FCN or from the Otsu's thresholding and Y denotes the foreground pixels of ground-truth.

2.4. *Pattern quantification*

Patterns obtained using the FCN were quantified. Connected-component labelling (CCL; Dillencourt et al., 1992) was first applied to the patterns for identifying the components (e.g., individual blobs) of the patterns. Subsequently, five traits were quantified for each ROI, namely mean component area, component quantity, primary area ratio, secondary area ratio, and logarithmic aspect ratio. The primary area ratio was defined as the ratio of the maximum component area in the ROI to ROI area. The secondary area ratio was defined as the ratio of the maximum component area in the ROI to total component area. The logarithmic aspect ratio was defined using three morphological properties of a component, namely major axis, minor axis, and orientation. Major and minor axes were the principal and secondary axes of the component obtained using CCL, respectively. The component orientation was defined as the angle between the image horizon and major axis of the component. For the component with an orientation between −45° and 45°, the aspect ratio was defined as the minor axis length to major axis length. Otherwise, the aspect ratio was defined as the ratio of the major axis length to minor axis length (Fig. 5). The logarithmic aspect ratio of a component was calculated as the binary logarithm of the aspect ratio of the component. A positive and negative logarithmic aspect ratio indicated the components with long and flat ellipse shapes, respectively. For each ROI, the distribution of the logarithmic aspect ratio was presented as a histogram. The trait differences between species were tested using Kruskal–Wallis test and Scheffé's multiple comparison tests (Scheffé, 1953).

2.5. *Colour trait quantification*

The colour traits of the ROI were quantified. Colour traits included the mean colour values of the ROI foreground (i.e., patterns) and background (Fig. 2d). The foreground and background colours are also referred to as the secondary

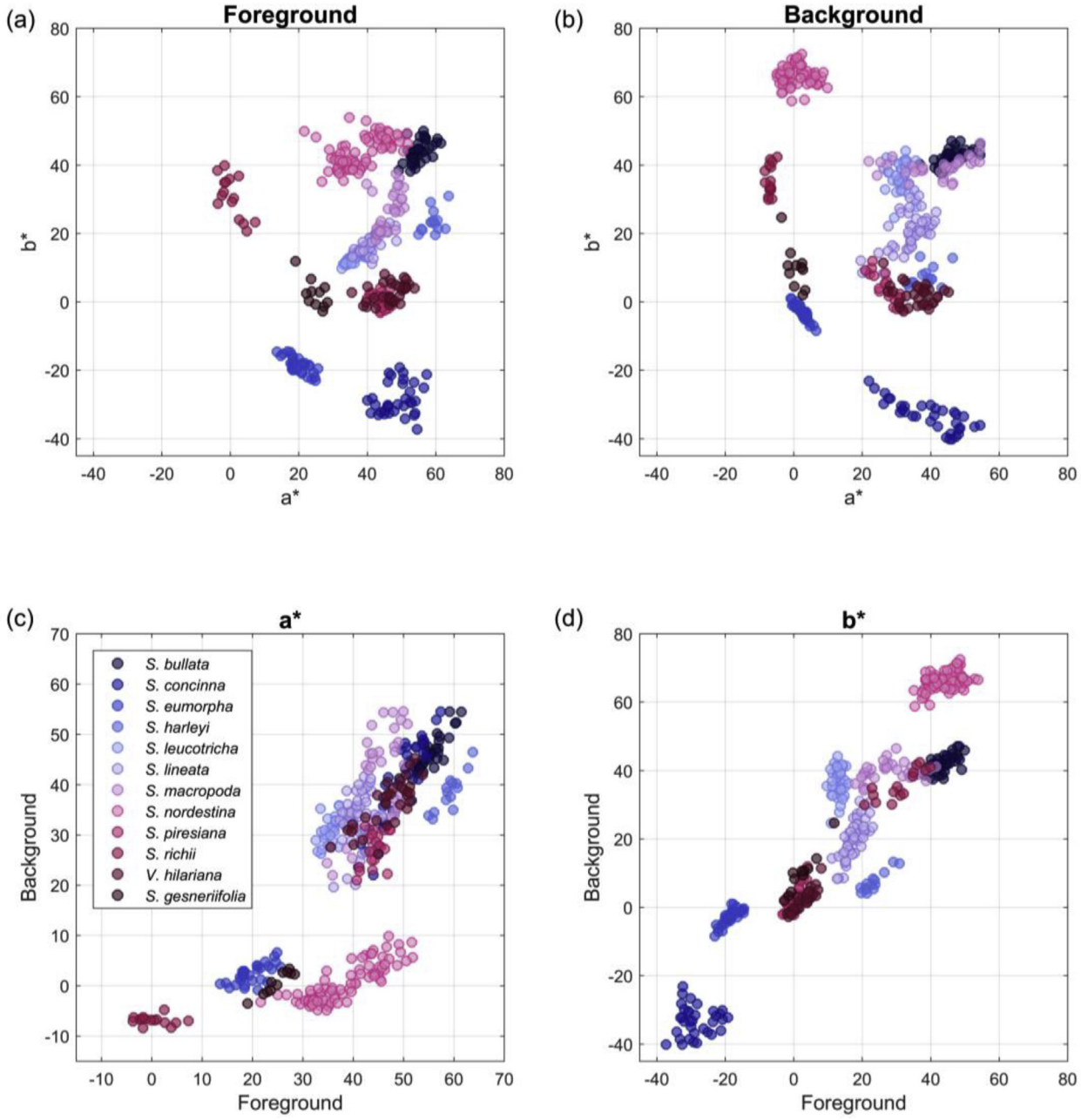

Fig. 9 – Mean (a) foreground and (b) background colours of *Sinningia* specimens in the a*–b* plane, and the (c) a* and (d) b* values of the foreground and background colours of *Sinningia* specimens.

and primary colours of the petals, respectively. The colours, obtained from the scanners and originally in RGB, were converted to CIE L*a*b* colour space, in which L*, a*, and b* represent lightness, redness, and blueness, respectively. The CIE L*a*b* colour parameters were pre-calibrated using a reference board (ColorChecker Passport, X-Rite; Grand Rapids, USA) and multiple regression (Hsu et al., 2018). Thus, the CIE L*a*b* colour parameters were device-independent.

3. Results

3.1. Pattern segmentation

The performance of the developed FCN was evaluated using the Dice score and the 33 test images (Fig. 6). The Dice score measures the similarity between two images. The FCN achieved a Dice score of 0.908, whereas Otsu's algorithm achieved a Dice score of 0.853. Patterns obtained using Otsu's algorithm exhibited noises in images with low contrast (*S. bullata*) and in the area of uneven petals (*S. eumorpha*). Although the FCN outperformed Otsu's algorithm, it could not achieve perfect segmentation in some images with similar foreground and background colours (*V. hilariana*).

3.2. Pattern traits

The variations in traits between the species were observed (Kruskal–Wallis test; Table 2). Figure 7 presents (a) the primary area ratio, (b) secondary area ratio, (c) mean component area, and (d) component quantity of each species. The species with plaque patterns (e.g., *S. leucitricha* and *S. piresiana*) were associated with large values in the primary ratio, secondary area ratio, and mean component area. The 50% primary area ratio served as an accurate demarcation for distinguishing plaque and "stripe and plaque" patterns (Fig. 7a). The 20% primary area ratio and 70% secondary area ratio served as demarcations for distinguishing "stripe and plaque" and stripe patterns (Fig. 7a and b). The results indicated that the cluster of proposed traits reflected the types of the pattern.

Figure 8 illustrates the logarithmic aspect ratios for each species. Differences in logarithmic aspect ratios among the petals of plaques, spots, and stripes were observed. The logarithmic aspect ratios for the species with plaque patterns (*S. leucotricha*) were bimodally distributed. By contrast, the logarithmic aspect ratios for the species with spot or stripe patterns were unimodally distributed. Also, the means of logarithmic aspect ratios for the species with only spot patterns (*S. concinna*, *V. hileriana*, and *S. gesneriifolia*) were lower than zero. By contrast, the means of logarithmic aspect ratios for the species with only stripe patterns (*S. eumorpha* and *S. macropoda*) were larger than 1.5. For the species with both spot and stripe patterns, the means of logarithmic aspect ratios ranged between 0 and 1.5. It is worth to note that the species that contained more stripe patterns than spot patterns (e.g., *S. bullata* and *S. nordestina*) had the means of logarithmic aspect ratios close to 1.5. By contrast, the species that contained more spot patterns than stripe patterns (e.g., *S. lineata* and *S. harleyi*) had the means of logarithmic aspect ratios close to zero.

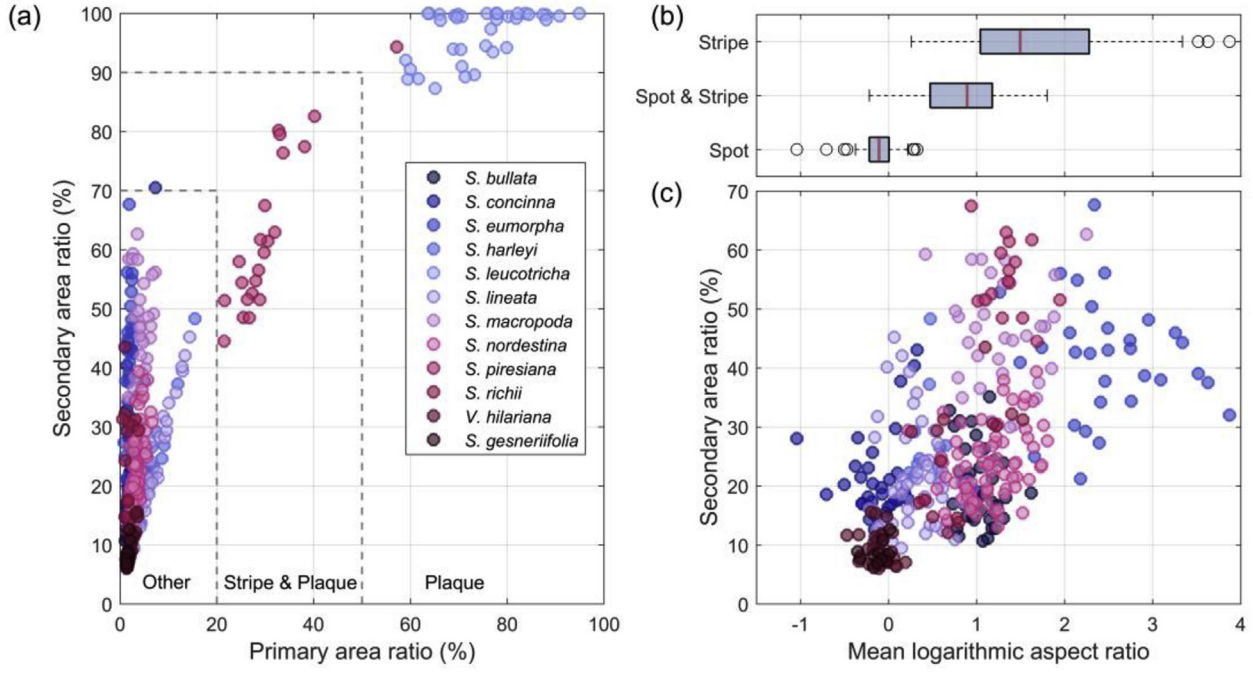

Fig. 10 – (a) *Sinningia* specimens in the trait space of the primary area ratio and secondary area ratio, (b) boxplots of spot, "spot and stripe", and stripe in mean logarithmic aspect ratio, and (c) *Sinningia* specimens in the trait space of the mean logarithmic aspect ratio and secondary area ratio.

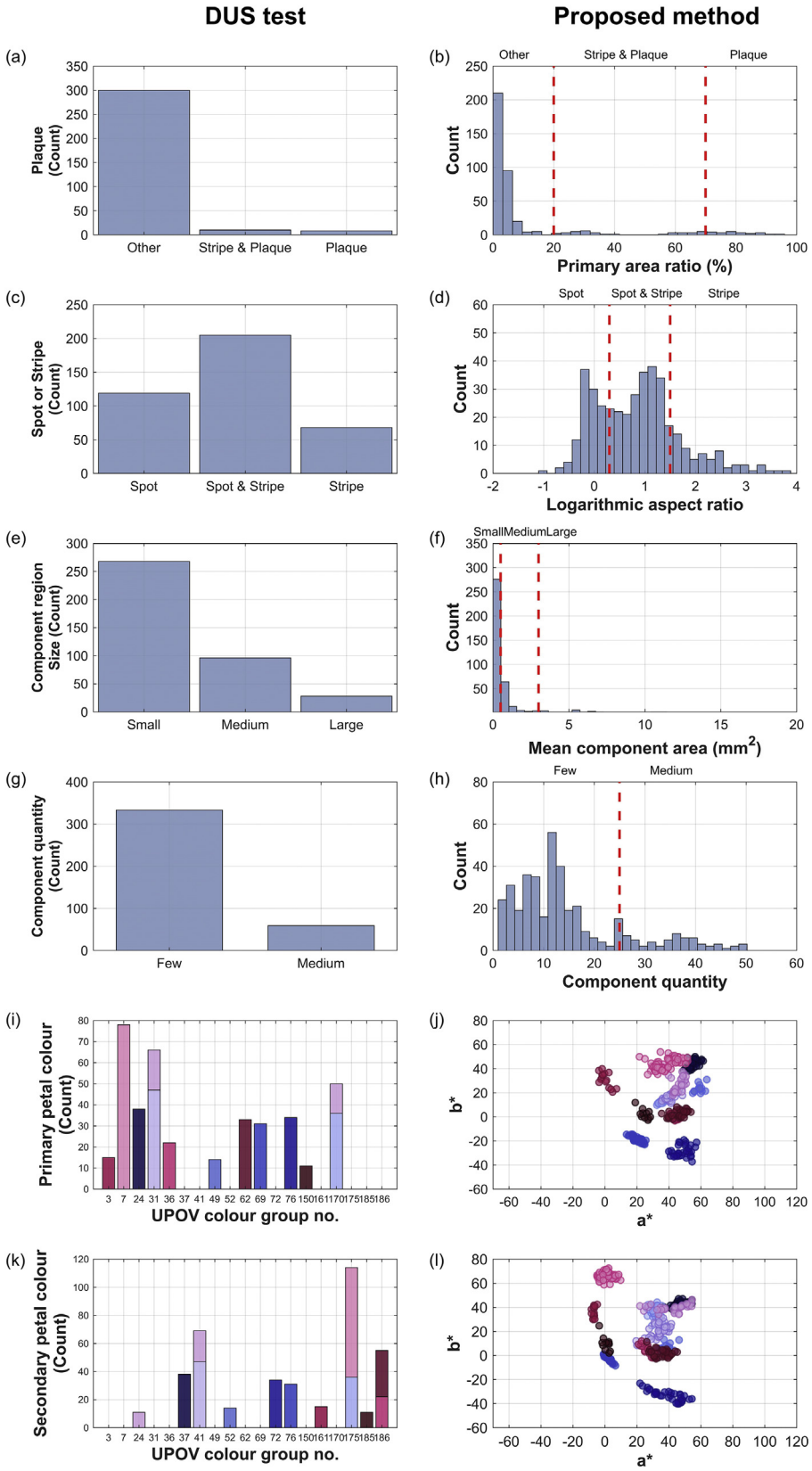

Fig. 11 – Comparison between the DUS test and proposed method in quantifying: (a) (b) plaque, (c) (d) spot or stripe, (e) (f) component region, (g) (h) component quantity, (i) (j) primary colour, and (k) (l) secondary colour. The red dashed lines in (b), (d), (f), and (h) correspond to the boundaries of the trait levels in the DUS test.

3.3. Colour traits

The mean foreground and background colours of the specimens in the a*–b* plane were examined. a* represents the green–red channel and b* represents blue–yellow channel. The ranges of the mean foreground colour were between −3.37 and 63.77, and −37.77 and 53.87 in a* and b*, respectively (Fig. 9a). The ranges of the mean background colour were between −8.41 and 54.52, and −40.14 and 72.41 in a* and b*, respectively (Fig. 9b). Furthermore, correlations between the mean foreground and background colours were examined (Figs. 9c and d). The mean foreground and background colours were strongly correlated in the a* and b* channels ($r = 0.72$ and $r = 0.92$, respectively). The strong correlation indicated that the foreground and background colours may contain similar pigments with different concentrations within a species.

3.4. Pattern distribution in the trait space

The patterns of each ROI in the trait space of the primary area ratio, secondary area ratio, and mean logarithmic aspect ratio are presented in Fig. 10. The figure shows that the specimens were distributed in the space continuously. Clear thresholds that differentiated the petals with the patterns of plaque, stripe and plaque, and "other" in the primary area and secondary area ratios were observed (Fig. 10a). The petals with the patterns of "other" can be further categorised into spot, "spot and stripe", and stripe using the mean logarithmic aspect ratio (Fig. 10b and c). These observations indicated that proposed traits can be effectively used to classify petals.

3.5. Application to new flower variety examination

The proposed method for quantifying petal traits can improve the precision in petal classification. Flowers are generally classified according to distinctness, uniformity, and stability (DUS) guideline (UPOV, 2015). Figure 11 presents the quantification and classification of 392 petal specimens conducted using the conventional DUS test and proposed method. The DUS test is typically performed by observing with the naked eye. Thus, the DUS test categorised four pattern traits (plaque, spot or stripe, component region, and component quantity) into only two or three classes (Figs. 11a, c, 11e, and 11g). By contrast, the proposed method could quantitatively evaluate the traits (Figs. 11b, d, 11f, and 11h). For comparison purpose, the thresholds used for categorizing the petals in the DUS test were identified and annotated as red lines in the figures of the proposed method (Figs. 11b, d, 11f, and 11h). The thresholds were not uniformly distributed in the space of the pattern traits. This observation suggests that the proposed method could be used to fill the gap between the thresholds of the conventional DUS test. The DUS test categorised the primary and secondary colours of petals into 19 groups using the RHS colour chart (Figs. 11i and k). By contrast, the proposed method accurately quantified the primary and secondary colour in the CIE L*a*b* parameters (Figs. 11j and l).

4. Conclusion

The study proposed a method to quantify petal patterns and colours for 11 *Sinningia* species. The ROI was first defined in the ventral petal containing the most versatile pattern and colour traits. Patterns in the ROI were then segmented using the FCN. Subsequently, petal pattern and colour traits were quantified using image processing. The trained FCN outperformed the conventional Otsu's method in pattern segmentation. The proposed method can quantify petal traits precisely and objectively and can be used to assist the automation of petal pattern rating, which is generally performed using naked-eye observation and DUS test.

Declaration of Competing Interest

The authors declare that they have no known competing financial interests or personal relationships that could have appeared to influence the work reported in this paper.

Acknowledgments

This research was supported by NSC-101-2313-B-002-050-MY3 from the Ministry of Science and Technology (former National Science Council), Taiwan. We thank Dr. Der-Ming Yeh at the National Taiwan University for constructive suggestions for this research and Mr. Chun-Ming Chen at the Dr. Cecilia Koo Botanic Conservation and Environmental Protection Centre for providing the plant materials.

Nomenclature

a*	Redness
b*	Blueness
CCL	Connected-component labelling
DUS test	The distinctness, uniformity, and stability test
FCN	Fully convolutional network
L*	Lightness
KBCC	Dr. Cecilia Koo Botanic Conservation Center
RGB	red, green, and blue
RHS	The Royal Horticultural Society
ROI	Region of interest
UPOV	International Union for the Protection of New Varieties of Plants

REFERENCES

Badrinarayanan, V., Handa, A., & Cipolla, R. (2015). Segnet: A deep convolutional encoder-decoder architecture for robust semantic pixel-wise labelling. *arXiv preprint arXiv:1505.07293*.

Biradar, B. V., & Shrikhande, S. P. (2015). Flower detection and counting using morphological and segmentation technique. *International Journal of Computer Science & Information Technology, 6*, 2498–2501.

Chen, J., Fan, Y., Wang, T., Zhang, C., Qiu, Z., & He, Y. (2018). Automatic segmentation and counting of aphid nymphs on

leaves using convolutional neural networks. *Agronomy, 8*(8), 129.
De Keyser, E., Lootens, P., Van Bockstaele, E., & De Riek, J. (2013). Image analysis for QTL mapping of flower colour and leaf characteristics in pot azalea (Rhododendron simsii hybrids). *Euphytica, 189*(3), 445–460.
Dice, L. R. (1945). Measures of the amount of ecologic association between species. *Ecology, 26*(3), 297–302.
Dillencourt, M. B., Samet, H., & Tamminen, M. (1992). A general approach to connected-component labeling for arbitrary image representations. *Journal of the ACM (JACM), 39*(2), 253–280.
Fawakherji, M., Youssef, A., Bloisi, D., Pretto, A., & Nardi, D. (2019, February). Crop and weeds classification for precision agriculture using context-independent pixel-wise segmentation. In *2019 third IEEE international conference on robotic computing (IRC)* (pp. 146–152). IEEE.
Garcia, J. E., Greentree, A. D., Shrestha, M., Dorin, A., & Dyer, A. G. (2014). Flower colours through the lens: Quantitative measurement with visible and ultraviolet digital photography. *PloS One, 9*(5), Article e96646.
Glorot, X., Bordes, A., & Bengio, Y. (2011, June). Deep sparse rectifier neural networks. In *Proceedings of the fourteenth international conference on artificial intelligence and statistics* (pp. 315–323).
Guo, Z., Zhang, L., & Zhang, D. (2010). A completed modeling of local binary pattern operator for texture classification. *IEEE Transactions on Image Processing, 19*(6), 1657–1663.
Hanbury, A., & Serra, J. (2001). *Mathematical morphology in the L* a* b* colour space*. Perancis: Centre de Morphologie Mathématique Ecole des Mines de Paris.
Haralick, R. M., & Shanmugam, K. (1973). Textural features for image classification. *IEEE Transactions on systems, man, and cybernetics*, (6), 610–621.
Hsu, H. C., Hsu, K. L., Chan, C. Y., Wang, C. N., & Kuo, Y. F. (2018). Quantifying colour and spot characteristics for the ventral petals in Sinningia speciosa. *Biosystems Engineering, 167*, 40–50.
Hung, T. T., Hsu, H. C., & Kuo, Y. F. (2019). Quantifying color and textural patterns of petals and studying their association with pollinators: Using genus Sinningia (GESNERIACEAE) as an example. In *2019 ASABE annual international meeting* (p. 1). American Society of Agricultural and Biological Engineers.
Iljazi, J. (2017). *Deep learning for image-based prediction of plant growth in City Farms* (Master's thesis). Eindhoven University of Technology.
Inthiyaz, S., Madhav, B. T. P., & Kishore, P. V. V. (2017). Flower segmentation with level sets evolution controlled by colour, texture and shape features. *Cogent Engineering, 4*(1), 1323572.
Ioffe, S., & Szegedy, C. (2015). Batch normalization: Accelerating deep network training by reducing internal covariate shift. *arXiv preprint arXiv:1502.03167*.
Kendal, D., Hauser, C. E., Garrard, G. E., Jellinek, S., Giljohann, K. M., & Moore, J. L. (2013). Quantifying plant colour and colour difference as perceived by humans using digital images. *PloS One, 8*(8), Article e72296.
Kingma, D. P., & Ba, J. (2014). Adam: A method for stochastic optimization. *arXiv preprint arXiv:1412.6980*.
Kitagawa, D., Mochizuki, Y., & Kobayashi, T. (2004). *U.S. Patent No. 6*. Washington, DC: U.S: Patent and Trademark Office.
Koski, M. H., & Ashman, T. L. (2013). Quantitative variation, heritability, and trait correlations for ultraviolet floral traits in Argentina anserina (Rosaceae): Implications for floral evolution. *International Journal of Plant Sciences, 174*(8), 1109–1120.
Lameski, P., Zdravevski, E., Trajkovik, V., & Kulakov, A. (2017, September). Weed detection dataset with RGB images taken under variable light conditions. In *International conference on ICT innovations* (pp. 112–119). Cham: Springer.
Long, J., Shelhamer, E., & Darrell, T. (2015). Fully convolutional networks for semantic segmentation. In *Proceedings of the IEEE conference on computer vision and pattern recognition* (pp. 3431–3440).
Najjar, A., & Zagrouba, E. (2012, June). Flower image segmentation based on color analysis and a supervised evaluation. In *2012 international conference on communications and information Technology (ICCIT)* (pp. 397–401). IEEE.
Nasios, N., & Bors, A. G. (2006). Variational learning for Gaussian mixture models. *IEEE Transactions on Systems, Man, and Cybernetics, Part B (Cybernetics), 36*(4), 849–862.
Noh, H., Hong, S., & Han, B. (2015). Learning deconvolution network for semantic segmentation. In *Proceedings of the IEEE international conference on computer vision* (pp. 1520–1528).
Odena, A., Dumoulin, V., & Olah, C. (2016). Deconvolution and checkerboard artifacts. *Distill, 1*(10), e3.
Otsu, N. (1979). A threshold selection method from gray-level histograms. *IEEE Transactions on Systems, Man, and Cybernetics, 9*(1), 62–66.
Paszke, A., Gross, S., Chintala, S., Chanan, G., Yang, E., DeVito, Z., Lin, Z., Desmaison, A., Antiga, L., & Lerer, A. (2017). Automatic differentiation in pytorch. In *31st conference on neural information processing systems (NIPS 2017), Long Beach, CA, USA*.
Patil, A. B., & Shaikh, J. A. (2016). OTSU thresholding method for flower image segmentation. *International Journal of Computational Engineering Research (IJCER), 6*(5).
Perret, M., Chautems, A., Spichiger, R., Barraclough, T. G., & Savolainen, V. (2007). The geographical pattern of speciation and floral diversification in the neotropics: The tribe Sinningieae (Gesneriaceae) as a case study. *Evolution: International Journal of Organic Evolution, 61*(7), 1641–1660.
Ronneberger, O., Fischer, P., & Brox, T. (2015, October). U-net: Convolutional networks for biomedical image segmentation. In *International Conference on Medical image computing and computer-assisted intervention* (pp. 234–241). Cham: Springer.
Scheffé, H. (1953). A method for judging all contrasts in the analysis of variance. *Biometrika, 40*(1–2), 87–110.
Srivastava, N., Hinton, G., Krizhevsky, A., Sutskever, I., & Salakhutdinov, R. (2014). Dropout: A simple way to prevent neural networks from overfitting. *Journal of Machine Learning Research, 15*(1), 1929–1958.
UPOV. (2015). *TG/283/1*. International Union for the Protection of New Varieties of Plants.
Van Den Boomgaard, R., & Van Balen, R. (1992). Methods for fast morphological image transforms using bitmapped binary images. *CVGIP: Graphical Models and Image Processing, 54*(3), 252–258.
Voss, D. H. (1992). Relating colorimeter measurement of plant color to the royal horticultural society colour chart. *HortScience, 27*(12), 1256–1260.
Yoshioka, Y., Ohsawa, R., Iwata, H., Ninomiya, S., & Fukuta, N. (2006). Quantitative evaluation of petal shape and picotee color pattern in lisianthus by image analysis. *Journal of the American Society for Horticultural Science, 131*(2), 261–266.